VOL. 10, NO. 18, OCTOBER 2015 ISSN 1819-6608
ARPN Journal of Engineering and Applied Sciences

www.arpnjournals.com

DETERMINATION OF YOUNG'S MODULI OF CLAYS USING IMAGE PROCESSING TECHNIQUE AND STRESS-STRAIN CALCULATION

Riska Ekawita[1], Eko Widiatmoko[1], Hasbullah Nawir[2], Suprijadi[3] and Khairurrijal[1]
[1]Physics of Electronic Materials Research Division, Faculty of Mathematics and Natural Sciences, Bandung, Indonesia
[2]Geotechnical Engineering Research Division, Faculty of Civil and Environmental Engineering, Bandung, Indonesia
[3]Theoretical High Energy Physics and Instrumentation Research Division, Faculty of Mathematics and Natural Sciences, Institut Teknologi Bandung, Jalan Ganesa, Bandung, Indonesia
E-Mail: krijal@fi.itb.ac.id

ABSTRACT

A system that consists of compression, imaging, and computation subsystems was successfully developed to determine Young's moduli of clay samples. The compression subsystem utilized a Mark-10 instrument that has a compressor with a capacity of 11.3 Nm. The instrument also has a displacement sensor with a resolution of 0.01 mm and an integrated display that was used as a standard to compare deformations obtained from images. The imaging subsystem operated a Canon IVX digital camera to obtain images with sizes of 3000×4000 pixels. The computation subsystem exploited a personal computer (PC) installed with Scilab ver. 5.3.3 to process the images. Experimentally, a clay sample was initially prepared in cylindrical shape. The sample was then continuously compressed at the rate of 80 mm/min and its image was subsequently captured every second. Next, the obtained images were processed to extract deformation experienced by the sample. Finally, the sample deformation was used to calculate its Young's modulus. It was shown that deformation data obtained from image processing are almost the same as those recorded by the Mark-10 display with the coefficient of determination R2 of 0.99. As the accurate displacement sensor is much more expensive than the Canon IVX digital camera, the image processing technique offers an affordable way to obtain deformation. It was demonstrated that Young's modulus versus the quadratic of height has very good linearity as revealed by the R2 coefficient of 0.94. This result is in agreement with the theoretical formula.

Keywords: compression, image processing, deformation, Young's modulus.

INTRODUCTION

Elastic modulus, which is also known as Young's modulus, of soil is one property that is difficult to estimate because it depends on many factors, such as the state of soil and the loading process. In other fields, many methods were already established to measure Young's moduli of various materials. Cone penetration test was used to determine Young's modulus of cemented sand [1] and micro-Raman spectroscopy was employed to evaluate that of carbon nanotube [2]. Moreover, atomic force microscope [3], ultrasound-stimulated acoustic emission imaging [4] and image processing [5] were utilized for obtaining Young's moduli of soft materials, tissues, and bones, respectively.

On the other hand, image processing methods, which are often applied to assess changes in a dimension of an object, develop quickly due to security [6], time, and reduced human error on data reading [7]. They are employed in diverse fields of science for numerous purposes or various applications. In agricultural science, for instance, image processing was utilized to get information on plant growth [8], percentage of weeds, crops [9], moisture content of rough rice [10], and wood pore identification [11]. Some applications include early detection and treatment of cancer [12] and quantization and flow of red blood cells [13] in medical science.

Other applications of image processing can also be found in the field of soil engineering to analyze soil properties such as microstructures and soil strength [14-17]. In this paper we describe a technique to determine Young's moduli of clay samples using a combination of image processing technique and stress-strain calculation. A clay sample will initially be prepared in cylindrical shape. Then, the sample will be continuously compressed at a certain rate and its image will be captured at a certain time interval. Next, the obtained image will be processed to extract deformation experienced by the sample. In order to examine the accuracy of deformations that were extracted from the images, a highly accurate deformation sensor of Mark-10 instrument will be employed as a standard and a vernier caliper as a supplementary standard. Finally, the sample deformation will be used to calculate its Young's modulus.

EXPERIMENTAL SETUP

Figure-1 gives the block diagram of a system developed for determining Young's modulus of clay samples. It consisted of compression, imaging, and computation subsystems. The compression subsystem employed a Mark-10 instrument which has a compressor with a capacity of 11.3 Nm to compress a cylindrical solid sample. The instrument has an accurate displacement sensor with a resolution of 0.01 mm and an integrated display that was used as a standard to assess deformations obtained from image processing. The imaging subsystem used a Canon IVX digital camera to obtain images with sizes of 3000×4000 pixels. A high quality image was got by the help of a fluorescent lamp that eliminates shadows. The camera and the lamp were positioned at 250 mm in front of the sample. In order to discriminate the image of clay sample, blue background and green plates were applied. This location was set by trial and error until the

images were good with no shadow. The computation subsystem utilized a personal computer (PC) that was installed with Scilab ver. 5.3.3 to process the images.

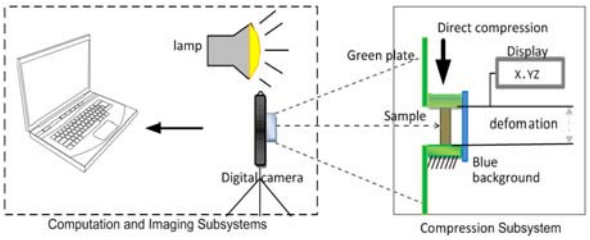

Figure-1. Experimental set up.

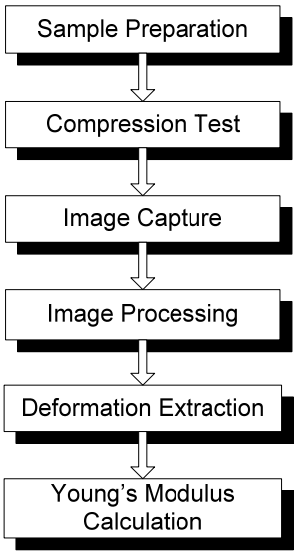

Figure-2. Experimental procedure performed to determine Young's modulus of the clay sample.

The experimental procedure, which starts from the clay sample preparation and ends to the calculation of its Young's modulus, is illustrated in Figure-2. First, a clay sample was prepared in cylindrical shape. The sample was then continuously compressed by employing the compression subsystem at the rate of 80 mm/min. Its image was then captured by utilizing the imaging subsystem every second. Next, the computation subsystem processed the image to extract deformation experienced by the sample. The deformation extracted from the image was compared to that measured by the deformation sensor of Mark-10 instrument or a vernier caliper. Finally, the sample deformation was applied to calculate its Young's modulus.

IMAGE PROCESSING AND DEFORMATION EXTRACTION

Image processing performed in the computation subsystem to extract clay sample deformation was divided into 3 main steps: a) uploading images into Scilab, b) converting pixels into millimeter unit, and c) determining the sample height. First, a series of images were put into the workspace available in Scilab. A script was written to speed up the analyzing process of the images.

Next, the conversion process of pixels of an image into a millimeter unit was performed. A vernier caliper that has main scale markings with dark colors and a bright color between 2 consecutive scales/dark colors were located close to the left of the orange area border at a fixed distance. Then, a column of pixels were read from the image, which contains an alternating dark and bright pattern that corresponds to one-millimeter scale of the caliper. By applying the Fast Fourier Transform (FFT) to this pixel column, the period of the pattern in pixels were calculated from the most prominent frequency component in the FFT result, excluding the two lowest frequencies and the upper half. This conversion process was repeated for all images.

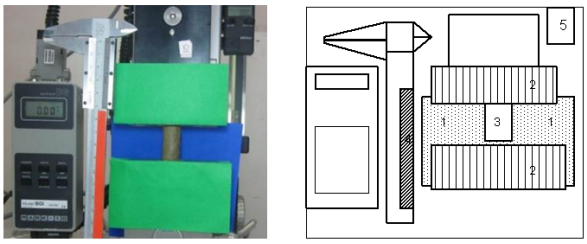

(a) (b)

Figure-3. (a) An image of a clay sample compressed by the compression subsystem and (b) Schematic description of the image.

For the purpose of determining clay sample height, sample boundaries in the image must be first traced. The selection of an appropriate method for tracing sample boundaries greatly affects measured values of the sample boundaries. A method that can be used to detect sample boundaries is segmentation, which consists of two approaches: edge and region segmentations [15]. We applied the edge segmentation approach with a threshold method for each image. Figure-3(a) gives an image in JPEG format of a clay sample that will be processed to find its boundaries. Referring to Figure-3(b), the image shown in Figure-3.(a) is composed of the blue background (label 1), which is placed behind the clay sample (label 3), and the green foreground (label 2), which is located on the compression plates of the compression subsystem. They make easier to find vertical edges (left and right edges) and horizontal edges (top and bottom edges) of the sample. An orange band (label 4) is attached next to the main scale of caliper functions as a "scale bar" to obtain a height of the image, so that the deformation obtained by the image can be compared with that measured by the Mark-10 as shown by its display (label 5).

YOUNG'S MODULUS CALCULATION

Young's modulus E is defined as the ratio of tensile stress to extensional strain experienced by a sample. Since the tensile stress due to the force F applied to an area A of the sample and the extensional strain due

to an extension dL of the height L are given by F/A and dL/L, respectively, Young's modulus can be expressed as Eq. (1).

$$E = \frac{stress}{strain} = \frac{(F/A)}{(dL/L)} \quad (1)$$

By employing image processing to a sample, an extension dL of the height L and the width of a sample are determined. Young's modulus of the sample can therefore be calculated. As an image of a sample will be captured every second, Young's modulus of the sample will be a function of time.

Previous researchers have found experimentally that some factors affected Young's modulus of a material. The factors are time [18-19], magnetic field [20] and humidity [21]. Chou *et al*. have observed the effect of a time thermal shock treatment to the Young's modulus of polycrystalline Yttrium Iron Garnet (YIG), the longer the time, the higher the modulus. On testing of soil samples, the increase of the consolidation time will make Young's moduli higher. The magnetic field can also increase Young's moduli as observed in electrodeposited NiFe and NiFeCo microtubes. Young's moduli of proton exchange membrane fuel cell electrodes decrease when the humidity around the electrodes becomes higher. On the other hand, another researcher has showed computationally that Young's modulus of a material can be influenced by its size [22]. By enlarging the diameter of single-walled carbon nanotubes, its Young's modulus becomes higher.
For soft clay, the effect of sample compression to its Young's modulus is given in Eq. (2).

$$E = \rho\left(\frac{2\pi f_n H}{\beta}\right)^2 \quad (2)$$

where E is Young's modulus, ρ is the density of sample, fn is the free vibration frequency of sample, H is the height of sample and β can be obtained as follows:

$$\beta . tg\beta = \frac{I}{I_0} \cdot \quad (3)$$

Here, I_0 is the polar moment of inertia of additional mass with the value of 24.529 kg•cm2 and I is the sample polar moment of inertia.

EXPERIMENTAL RESULTS AND DISCUSSIONS

Clays originated from seafloor sediments of East Kalimantan and North Sumatera, Indonesia, were made as samples to verify the method. Samples were prepared in cylindrical shapes with 30 mm in height and 15 mm in diameter from the as-received clays. Figure-4 depicts the samples made of clays of East Kalimantan (samples #1 and #2) and North Sumatera (samples #3 and #4).

Figure-4. Clay samples from seafloor sediments of East Kalimantan (a) and North Sumatera (b), Indonesia.

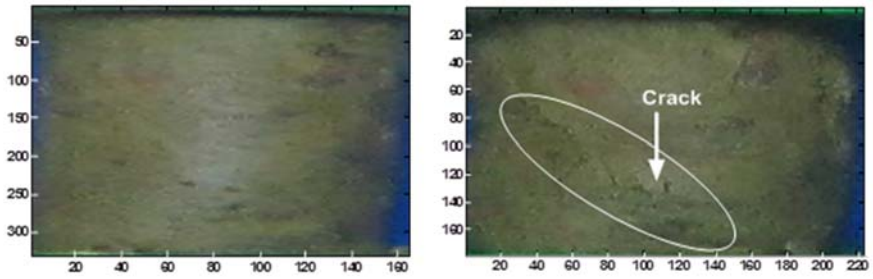

(a) (b)

Figure-5. Images of sample #1 (a) before compression, (b) after compression and crack.

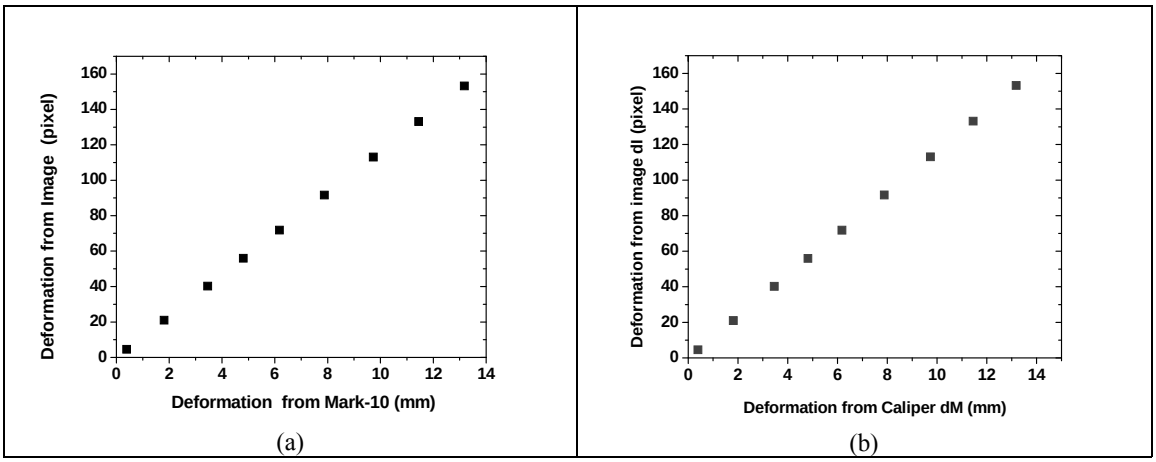

Figure-6. Correlation between deformations in pixel and mm units obtained from either the vernier caliper or the Mark-10.

A force generated by the compression subsystem was applied to squeeze a sample. In the case of sample #1, the sample started cracking at the force of 0.04 kN and the compression was stopped at this moment. Figure-5 presents two processed images of sample #1: (a) before compression and (b) after compression and crack. It was obtained that the height of original sample before compression is 333 pixels as shown in Figure-5(a). After the sample was compressed until crack, the cracked sample had a height of 180 pixels as given in Figure-5(b). Therefore, the maximum deformation of the sample was 153 pixels. By looking at the image of the orange band attached next to the main scale of vernier caliper, it was found that 1 mm equals to 11.62 pixels. Noting that the smallest unit of an image is one pixel, the resolution of an image is 1 mm/11.62 pixels or about 0.09 mm/pixel. It means that the resolution obtained from the image is the same as that given by the main scale of vernier caliper. Therefore, the vernier caliper is no longer required in determining deformation.

All images of the sample #1 compressed until it started cracking were recorded and the images were processed to obtain its deformation. The deformation in pixels obtained from a processed image is compared to those acquired from the caliper scale reading and the Mark-10 display as shown in Figure-6. The ordinate (y-axis) represents the deformation in pixel obtained by the image processing and the abscissa (x-axis) denotes the deformation in mm recorded by the Mark-10 display (Figure-6(a)) or read by the caliper (Figure-6(b)). It was found that the graphs give the deformation in pixels that increases linearly as increasing the deformation in mm (either using the caliper or Mark-10 display) and they have very good linearity as indicated by the coefficient of determination R2 of 1. Therefore, it implies that the caliper scale in the image can be used to convert pixel unit into mm unit for next measurements. These findings imply that deformations extracted from the images are comparable to those measured by the Mark-10 display or main scale of caliper. Consequently, images can independently be used to get deformations with good accuracy.

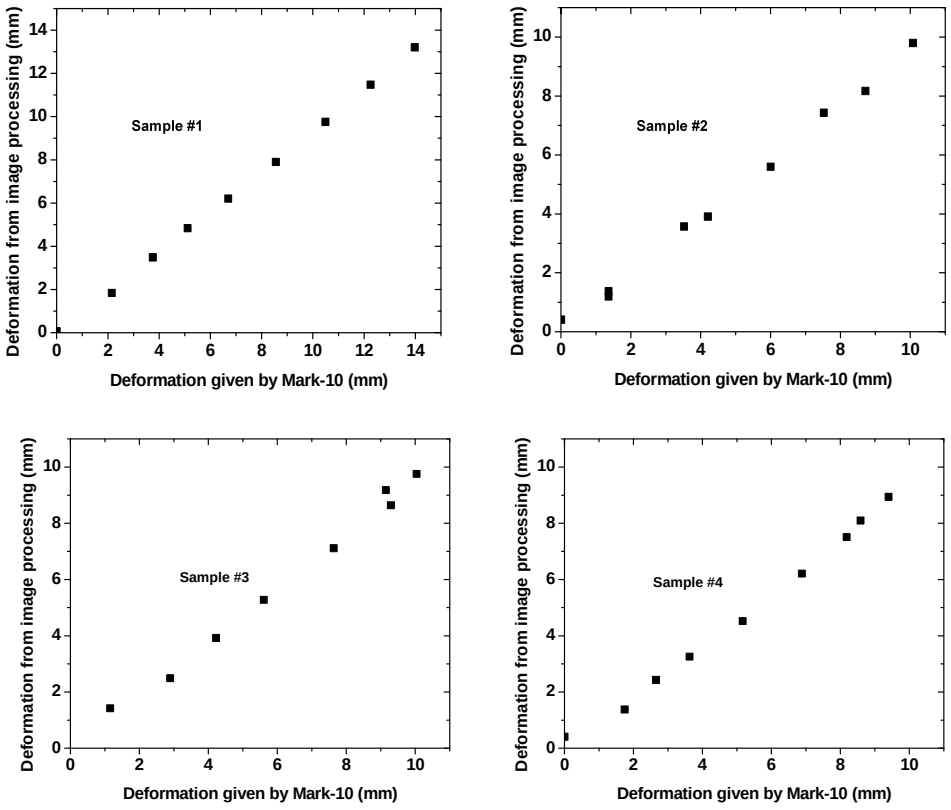

Figure-7. Deformation data in millimeters obtained from image processing and the Mark-10.

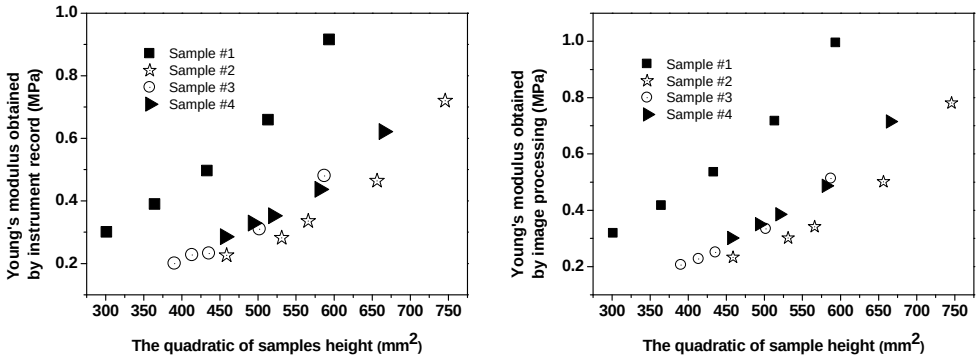

(a) (b)

Figure-8. Young's moduli of samples versus the quadratic of sample height.

In addition, deformation data recorded by the Mark-10 display were compared to those obtained from image processing after converting to mm unit with the method described before as shown in Figure-7. Among the samples, sample #1 has the best linearity with the maximum deviation 0.8 mm at the seventh point and the R2 coefficient of 0.999. While the minimum deviation of 0 mm was obtained in sample #3 at the seventh point. Sample #2 and sample #4 also have very good linearity as given by the R2 coefficients of 0.998 and 0.995, respectively. The differences may occur due to edges determination of the samples are still not quite well.

Table-1. Measured Height and Diameter and Calculated Young's modulus at every second.

Sample	Time (s)	Height (mm)	Diameter (mm)	F/A (kN/mm^2)	Instrument Record		Image Processing		
					dL/Lo	E (Mpa)	dL/Lo	E (Mpa)	
1	1	24.37	15.918	$20x10^{-5}$	0.22	0.914	0.202	0.994	
	2	22.67	16.606	$18x10^{-5}$	0.281	0.658	0.258	0.716	
	3	20.82	17.294	$17x10^{-5}$	0.344	0.495	0.318	0.535	
	4	19.1	18.069	$15x10^{-5}$	0.402	0.389	0.375	0.416	
	5	17.37	19.273	$13x10^{-5}$	0.458	0.299	0.431	0.318	Crack
2	1	27.31	16.176	$9.8x10^{-5}$	0.135	0.72	0.125	0.781	
	2	25.62	16.864	$8.9x10^{-5}$	0.193	0.464	0.179	0.501	
	3	23.79	17.725	$8.1x10^{-5}$	0.242	0.336	0.238	0.341	
	4	23.05	17.983	$7.9x10^{-5}$	0.28	0.282	0.261	0.302	
	5	21.42	18.671	$7.3x10^{-5}$	0.323	0.226	0.313	0.233	Crack
3	1	24.24	16.692	$9.1x10^{-5}$	0.191	0.48	0.178	0.513	
	2	22.41	17.811	$8.0x10^{-5}$	0.259	0.31	0.24	0.334	
	3	20.88	18.671	$7.3x10^{-5}$	0.316	0.232	0.292	0.25	
	4	20.34	19.015	$7.0x10^{-5}$	0.311	0.227	0.311	0.227	
	5	19.76	19.36	$6.8x10^{-5}$	0.341	0.2	0.33	0.206	Crack
4	1	25.79	15.488	$11 x10^{-5}$	0.171	0.621	0.149	0.715	
	2	24.1	16.004	$9.9x10^{-5}$	0.228	0.437	0.204	0.487	
	3	22.8	16.348	$9.5x10^{-5}$	0.271	0.352	0.247	0.386	
	4	22.21	16.52	$9.3x10^{-5}$	0.284	0.329	0.267	0.35	
	5	21.37	16.95	$8.9x10^{-5}$	0.311	0.285	0.294	0.301	Crack

These results indicate that highly accurate deformations are solely obtained from images. Because compression of a sample was uninterruptedly performed, manual deformation measurements using the vernier caliper became difficult. Moreover, the accurate deformation sensor is much more expensive so that the use of the deformation sensor is not reasonable. The application of widely used Canon IVX digital camera in obtaining deformations via images therefore solved the problems.

As a sample was continuously compressed at the rate of 80 mm/min and its image was captured every second before crack occurred, its Young's modulus, which was calculated by using Eq. (1), is then represented as a function of time of measurement as tabulated in Table-1. Inspecting data presented in Table 1, it is shown that the height and radius of every sample changes with time and calculated Young's modulus can be stated as a function of sample height as shown in Fig. 8. It is found that Young's modulus of a sample decreases as its height lowers. This occurred because the pore volume reduces and the sample density increases during the compression process [23]. Moreover, graphs of Young's modulus versus the quadratic of height have very good linearity as revealed by the R2 coefficients of 0.94 to 0.97. These findings agree very well with the theoretical formula given in Equation (2).

CONCLUSIONS

The combination of image processing technique (compression, imaging, and computation subsystems) and stress-strain calculation has been successfully developed to determine Young's moduli of clays. The compression subsystem utilized that of Mark-10 instrument, the imaging subsystem operated a Canon IVX digital camera, and the computation subsystem exploited Scilab ver. 5.3.3 on a personal computer. It has been shown that deformation data obtained from image processing were almost the same as those recorded by the Mark-10 display with the coefficient of determination R2 of 0.99. This finding confirmed that the image processing technique developed to obtain deformation data is consistent. In addition, it has also been found that the obtained Young's modulus is a function of the quadratic of sample height. This result is consistent with the theoretical formula.

ACKNOWLEDGEMENT

This work was funded by Directorate General of Higher Education, Ministry of Education and Culture of the Republic of Indonesia through "Desentralisasi ITB" Research Grant of the fiscal year 2012.

REFERENCES

[1] Lee M-J., Hong S-J., Choi, Y-M. and Lee W. 2010. Evaluation of deformation modulus of cemented sand

using CPT and DMT. Engineering Geology. 115: 28-35.

[2] Lourie O. and Wagner, H. D. 1998. Evaluation of young's modulus of carbon nanotubes by micro-raman spectroscopy. Journal of Materials Research. 13(9): 2418-2422.

[3] Dimitriadis E.K., Horkay, F., Maresca J., Kachar B. and Chadwick R.S. 2002. Determination of elastic moduli of thin layers of soft material using the atomic force microscope. Biophysical Journal. 82: 2798-2810.

[4] Konofagou E., Thierman J. and Hynynen K. 2003. The use of ultrasound-stimulated acoustic emission in the monitoring of modulus changes with temperature. Ultrasonic. 41(5): 337-345.

[5] Geraets W.G.M., Ruijven L.J.Van., Verheij J.G.C., Stelt P.F.Van der. and Eijden T.M.G.J. Van. 2008. Spatial orientation in bone samples and young's modulus. Journal of Biomechanics. 41: 2206-2210.

[6] Dworkin S.B. and Nye T.J. 2006. Image processing for machine vision measurement of hot formed parts. Journal of Materials Processing Technology. 174: 1-6.

[7] Zhou Y., Srinivasan R. and Lakshminarayanan S. 2009. Critical evaluation of image processing approaches for real time crystal size measurement. Computer and Chemical Engineering. 33: 1022-1035.

[8] Guijaro M., Pajares G., Riomoros I., Herrera P.J, Burgos-Artizzu X.P. and Ribeiro A. 2011. Automatic segmentation of relevant textures in agricultural images. Computers and Electronics in Agriculture. 75: 75-83.

[9] Burgos-Artizzu X.P., Ribeiro A., Tellaeche A., Pajares G. and Fernandez-Quintanilla C. 2010. Analysis of natural images processing for the extraction of agricultural elements. Image Vision Computing. 28: 138-149.

[10] Shei H-J. and Lin C-S. 2012. An optical automatic measurement method for the moisture content of rough rice using image processing techniques. Computers and Electronics in Agriculture. 85: 134-139.

[11] Pan S. and Kudo M. 2011. Segmentation of pores in wood microscopic images based on mathematical morphology with a variable structuring element. Computers and Electronics in Agriculture. 75: 250-260.

[12] Tang J., Rangayyan R., Yao J. and Yang Y. 2009. Digital image processing and pattern recognition techniques for the detection of cancer. Pattern Recognition. 42: 1015-1016.

[13] Higgins J. M., Eddington, D. T., Bhatia S. N. and Mahadevan L. 2009. Statistical dynamics of flowing red blood cells by morphological image processing. PLoS Computational Biology. 5(2): e1000288/1-10.

[14] Liu C., Shin B., Zhou J. and Tang C. 2011. Quantification and characterization of microporosity by image processing, geometric measurement and statistical methods: application on SEM image of clays materials. Applied Clay Science. 54: 97-106.

[15] Xu W-J., Xu Q. and Hu R-L. 2011. Study on the shear strength of soil rock mixture by large scale direct shear test. International Journal of Rock Mechanics and Mining Sciences. 48: 1235-1247.

[16] Qun Y., Jie S. and Xianbin D. 1992. Camera tracing and image processing system for soil deformation. Journal of Terramechanics. 29(4/5): 423-431.

[17] Bagherieh A.R., Habibagahi G. and Ghahramani A. 2008. A novel approach to measure the volume change of triaxial soil samples based on image processing. Journal of Applied Sciences. 8(13): 2387-2395.

[18] Binhui W., Guoxing C. and Jiyan Z. 2008. Effect of consolidation time on dynamic shear modulus of soft clay. The 14th World Conference on Earthquake Engineering Beijing China. pp. 1-8.

[19] Chou H.M. and Case E.D. 1988. Time-dependent recovery of the elastic modulus in thermally shocked polycrystalline yttrium iron garnet (YIG). Materials Science and Engineering. 100: 7-14.

[20] Atalay S., Atalay F.E. and Kaya H. 2007. Field dependent Young's modulus and magneto impedance in electrodeposited NiFe and NiFeCo microtubes. Journal of Magnetism and Magnetic Materials. 316: e805-e808.

[21] Lu Z., Santare M.H., Karlsson A.M., Busby F.C. and Walsh P. 2014. Time-dependent mechanical behavior of proton exchange membrane fuel cell electrodes. Journal of Power Sources. 245: 543-552.

[22] Fang S-C., Chang W-J. and Wang Y-H. 2007. Computation of chirality and size dependent surface Young's moduli for single-walled carbon nanotubes. Physics Letters A. 371: 499-503.

[23] Malik M.A., Ur-Rehman E., Naheed R. and Alam N.M. 2002. Pore volume determination by density of porous copolymer beads in dry state. Reactive and Functional Polymers. 50: 125-130.